Bone Reports 12 (2020) 100262

Contents lists available at ScienceDirect

Bone Reports

journal homepage: www.elsevier.com/locate/bonr

Radiation-induced changes to bone composition extend beyond periosteal bone

Gurjit S. Mandair[a], Megan E. Oest[b], Kenneth A. Mann[b], Michael D. Morris[c], Timothy A. Damron[b], David H. Kohn[a,d,*]

[a] School of Dentistry, University of Michigan, Ann Arbor, MI, USA
[b] Department of Orthopedic Surgery, Upstate Medical University, Syracuse, NY, USA
[c] Department of Chemistry, University of Michigan, Ann Arbor, USA
[d] Department of Biomedical Engineering, University of Michigan, Ann Arbor, USA

ARTICLE INFO

Keywords:
Post-irradiation
Mouse model
Raman spectroscopy
Bone quality
Cortical bone
Bone composition

ABSTRACT

Background: Cancer patients receiving radiotherapy for soft tissue sarcomas are often at risk of post-irradiation (post-RTx) bone fragility fractures, but our understanding of factors controlling radiation-induced bone injury is limited. Previous studies have evaluated post-RTx changes to cortical bone composition in the periosteum of irradiated tibiae, but have not evaluated effects of irradiation in deeper tissues, such as endosteal or mid-cortical bone, and whether there are differential spatial effects of irradiation. In this study, we hypothesize that post-RTx changes to cortical bone composition are greater in endosteal compared to mid-cortical or periosteal bone.

Methods: A pre-clinical mouse model of limited field hindlimb irradiation was used to evaluate spatial and temporal post-RTx changes to the metaphyseal cortex of irradiated tibiae. Irradiation was delivered unilaterally to the hindlimbs of 12-wk old female BALB/cJ mice as 4 consecutive daily doses of 5 Gy each. RTx and non-RTx tibiae were obtained at 0, 2, 4, 8, and 12 wks post-RTx (n = 9 mice/group/time). Raman spectroscopy was used to evaluate spatial and temporal post-RTx changes to cortical bone composition in age-matched RTx and non-RTx groups.

Results: Significant early spatial differences in mineral/matrix and collagen crosslink ratios were found between endosteal and periosteal or mid-cortical bone at 2-wks post-RTx. Although spatial differences were transient, mineral/matrix ratios significantly decreased and collagen crosslink ratios significantly increased with post-RTx time throughout the entire tibial metaphyseal cortex.

Conclusions: Irradiation negatively impacts the composition of cortical bone in a spatially-dependent manner starting as early as 2-wks post-RTx. Long-term progressive post-RTx changes across all cortical bone sites may eventually contribute to the increased risk of post-RTx bone fragility fractures.

1. Introduction

Radiotherapy treatments are intended to improve the clinical outcomes in cancer patients with soft tissue sarcomas but are also known to negatively alter bone structure and composition (Haas et al., 2018; de Baere et al., 2018). The severity of the bone alterations range from temporary bone loss, reduced growth and poor healing, to fragility fractures that may not occur until several months or years after the primary radiotherapy treatment (Oh and Huh, 2014; Jegoux et al., 2010; Hui et al., 2015). Post-irradiation (post-RTx) fragility fractures have been reported in urologic and gynecologic cancer patients with incidence levels of 8–14% (Oh and Huh, 2014; Baxter et al., 2005) and 7–19% (Kwon et al., 2008; Ikushima et al., 2006; Park et al., 2011), respectively. Breast cancer and sarcoma radiotherapy patients have also reported rib and femur fragility fractures with corresponding incidence levels of 8–21% (Helmstedter et al., 2001; Dickie et al., 2009) and 3–6% (Dunlap et al., 2010; Voroney et al., 2009). Given that two-thirds of cancer patients will undergo radiotherapy treatment alone or allied with other adjuvant therapies (Mattes et al., 2016; Chen and Kuo, 2017), there is a need to understand how radiotherapy alters bone structure, composition, and material strength. Such information would be helpful in optimizing current radiotherapy treatment programs designed to prevent the overloading of irradiated tissues and to rescue or prevent the occurrence of post-RTx fragility fractures (Shimoyama

* Corresponding author at: Departments of Biologic and Materials Sciences and Biomedical Engineering, University of Michigan, Ann Arbor, MI 48109-1078, USA.
E-mail address: dhkohn@umich.edu (D.H. Kohn).

https://doi.org/10.1016/j.bonr.2020.100262
Received 8 December 2019; Received in revised form 25 March 2020; Accepted 26 March 2020
Available online 28 March 2020

et al., 2017).

Pre-clinical mouse models of hindlimb irradiation have been used to study how changes in certain aspects of bone quality contribute towards fragility fractures (Oest and Damron, 2014; Oest et al., 2016; Green et al., 2013). For instance, transient increases in non-specific advanced glycation end-products, collagen pyridinoline and pentosidine cross-links in the femora of 4 × 5 Gy irradiated mice at 1-wk post-RTx, were proposed to explain bone matrix embrittlement and increased fracture risk (Oest and Damron, 2014). The quality of irradiated bone composition has also been evaluated by Raman spectroscopy, whereby tibiae from mice irradiated with a fractionated 4 × 5 Gy dose, exhibited increased trivalent-to-divalent collagen crosslink ratios, transient to persistent changes in mineral composition, and altered molecular orientation of bone mineral and collagen fibrils (Oest et al., 2016). However, only the periosteum of the tibiae was examined in this study. As such, little is known about the differential spatial effects of post-RTx in deeper tissues, such as mid-cortical or endosteal bone.

In this Raman spectroscopic study, we hypothesize that endosteal bone in the tibial metaphyseal cortex of female mice, irradiated with a fractionated 4 × 5 Gy dose, would exhibit the greatest spatial change in bone composition compared to mid-cortical or periosteal bone. This hypothesis is based on histomorphometric evidence of greater changes in endosteal mineral apposition rate with irradiation vs. periosteal (Oest et al., 2015), and endosteal bone formation rates being impaired to a greater degree in rodent models of aging (Silva et al., 2005), immobilization and cross-link inhibition (Weinreb et al., 1991). In addition, we examine how soon after limited field irradiation these changes manifest themselves, and whether these changes persist after the end of the study period at 12-wks post-RTx.

2. Materials and methods

2.1. Animal model and specimen preparation

All methods were approved by the SUNY Upstate Institutional Animal Care and Use Committee as described previously (Oest et al., 2016; Oest et al., 2018). Briefly, female BALB/cJ mice aged 12-wks were anesthetized and exposed to fractionated unilateral hindlimb limited field irradiation. Radiation was delivered as four consecutive daily fractions of 5 Gy each (4 × 5 Gy, n = 9 mice/group/time point). The non-irradiated hindlimbs served as an internal control (non-RTx). Mice were euthanized at 0, 1, 2, 4, 8, and 12-wks post-RTx. Both right (RTx, 4 × 5 Gy) and left (non-RTx, 0 Gy) tibiae were harvested, wrapped in saline-soaked gauze and frozen at −80 °C. Tibiae were transported overnight on dry ice to the University of Michigan and stored at −20 °C until required.

After thawing to ambient temperature, the fibula and surrounding non-osseous tissue were removed. The distal to mid-shaft region of each tibiae was wrapped in Teflon tape and parafilm, and secured inside a U-shaped Teflon holder, which allowed transverse sections to be created and polished in a reproducible manner. The tibiae were sectioned at the metaphysis using a diamond wafering blade (Model 650; South Bay Technology, San Clemente, CA) under constant irrigation (McNerny et al., 2015). The resulting transverse sections were rinsed with calcium buffered saline to remove any surface bone marrow blood or lipid residues. The bone marrow was then removed and the cortical surface lightly polished on wet silicon carbide paper (Grit 4000; Buehler, Lake Bluff, IL). The polished cortex was rinsed thoroughly with calcium buffered saline prior to multi-site sampling by Raman spectroscopy.

2.2. Raman spectroscopy

The Raman microscope used in this study has been described in detail elsewhere (Oest et al., 2016), but was modified to include a 785-nm diode laser (Innovative Photonics Solutions, Monmouth Junction, NJ) and a 25-μm slit to give a spectral resolution of ~4 cm^{-1} (Rux et al., 2017). The excitation laser was spot-focused through a 10×/0.50 *NA* objective (S Fluor; Nikon Instruments, Inc., Melville, NY) to give ~40 mW of laser power at the specimen. A low *NA* objective was used to minimize the polarization dependence of the bone mineral v_1PO_4 band at 959 cm^{-1}, owing to the intrinsic alignment of mineralized collagen fibers in bone (Oest et al., 2016; Raghavan et al., 2010; Kazanci et al., 2006; Kazanci et al., 2007).

The tibial specimen within the Teflon holder was secured upright on a standard microscope glass slide and then the entire assembly was mounted onto the microscope stage. The cortical surface was brought into focus. A series of spectra was then acquired from the endosteal, mid-cortical and periosteal surfaces at the lateral, medial, anterior, and posterior quadrants, to yield 12 spectra per tibia. Periosteal and endosteal measurement sites were defined as 5–10 μm from the inner and outer perimeter of the cortical section, respectively. This approach ensured that spectra were acquired in a reproducible manner with minimal interference from potential residual non-osseous tissue at the periosteum or blood and lipid residues at the endosteal bone/medullary interface. To ensure spectra were acquired with good signal-to-noise ratios and minimal background tissue fluorescence, the measurement sites were photobleached for 6 mins with the laser beam before the spectra were acquired using an accumulation cycle time of 6 min (2 × 3 min). All experiments were performed at room temperature with deionized water added to the bone surface at the beginning of each experiment. Wrapping the bones in Teflon tape and parafilm also minimized dehydration.

2.3. Data processing and spectral analysis

All Raman spectroscopic data were calibrated and processed in MatLab® software (The MathWorks, Inc., Natick, MA) using locally written scripts described elsewhere (Oest et al., 2016; Rux et al., 2017). The scripts included an automated '*adaptive min*-max' polynomial fitting sub-routine (3rd order, constrained) to correct for background tissue fluorescence (Cao et al., 2007). All spectra were imported into GRAMS/AI® software (Thermo Fisher Scientific, Madison, WI) for manual baseline correction (Kumar et al., 2016) and normalization against the symmetrical v_1 phosphate band at ~959 cm^{-1} (v_1PO_4) (Mandair and Morris, 2015; Mandair et al., 2018). For optimal curve-fitting, second derivative, and constrained Gaussian deconvolution functions were applied to the following spectral regions: 830–900 cm^{-1} (839, 853, 866, 876, and 889 cm^{-1}); 900–990 cm^{-1} (927, 943, and 959 cm^{-1}); and 1580–1714 cm^{-1} (amide-I sub-bands; 1586, 1597, 1605, 1616, 1625, 1634, 1644, 1653, 1665, 1680, 1688, and 1701 cm^{-1}) (Mandair and Morris, 2015; Orkoula et al., 2012). Raman bands relevant to bone were identified: proline (Pro) and hydroxyproline (Hyp) bands at ~853 cm^{-1} and ~876 cm^{-1}, respectively; amide I sub-bands at ~1665 cm^{-1} (trivalent collagen crosslink) and ~1680 cm^{-1} (divalent collagen crosslink) (Oest et al., 2016; McNerny et al., 2015; Mandair and Morris, 2015). The amide-I peak-fit model contained an additional band at ~1653 cm^{-1} (lipid $\nu(C{-}C)_{cis}$ vibration (Penel et al., 2005) with minor collagen amide I contribution) to correct for any potential lipid interference to the adjacent trivalent collagen crosslink band at ~1665 cm^{-1} (Mandair and Morris, 2015; Penel et al., 2005). The following select Raman compositional parameters for cortical bone were calculated: Mineral/matrix ratio (959/(853 + 876) cm^{-1}) (Oest et al., 2016; McNerny et al., 2015); Hyp/Pro ratio (876/853 cm^{-1}) (Burke et al., 2016; Unal et al., 2018a); and collagen crosslinks ratio (1665/1680 cm^{-1}) (McNerny et al., 2015; Orkoula et al., 2012; Gong et al., 2013). Mineral/matrix ratio is related to the amount of mineral within a given volume of bone matrix analyzed and is positively correlated with tissue mineral density (Shi et al., 2018), ash weight (Taylor et al., 2017), and has also been validated against synthetic bio-apatite standards (Karampas et al., 2013). Collagen crosslinks ratios were extrapolated from earlier spectroscopic studies (Oest et al., 2016; McNerny et al., 2015; Paschalis et al., 2001) and are considered to reflect the

relative ratio of the mature trivalent (pyridinoline) crosslink to the immature divalent (dehydrodihydroxylysinonorleucine) crosslink. The Hyp/Pro ratio provides an indirect measure of post-translational modifications to collagen (Burke et al., 2016; Unal et al., 2018a). The mineral crystallinity parameter is the inverse of the full-width at half maximum (1/FWHM) of the Gaussian-fitted v_1PO_4 band at 959 cm^{-1} (Mandair et al., 2018), and is correlated with mineral crystal size measurements from X-ray diffraction (Sa et al., 2017).

2.4. Statistical analysis

Statistical analyses were performed in SPSS Statistics Software for Windows (IBM SPSS Statistics Version 24, IBM Corp., NY). For each compositional parameter, mean values were calculated for endosteal, mid-cortical and periosteal bone surfaces, including the pooled mean compositional values obtained by averaging the measurements from across all three bone surfaces. For graphical display, the mean differences between RTx and non-RTx groups were first converted into percentage differences for a given compositional parameter. Box and whisker plots were then used to display the median percentage differences for each compositional parameter as a function of bone surface (periosteal, mid-cortical, endosteal, or pooled) and time point (0, 1, 2, 4, 8, or 12-wks post-RTx). First, statistically significant percentage differences in composition between RTx and non-RTx groups by bone surface and time point were calculated using the pairwise related-samples Wilcoxon signed rank test ($p < 0.05$). Second, statistically significant pairwise spatial percentage differences in composition between endosteal, mid-cortical, or periosteal bone surfaces across multiple time points (0, 1, 2, 4, 8, and 12-wks post-RTx) were then calculated using the nonparametric Kruskal-Wallis one-way ANOVA multi-group comparison test ($p < 0.05$). Similarly, borderline to significant spatial differences between bone surfaces were also calculated for RTx and non-RTx experimental groups, with select p-values as indicated in the box and whisker plots. Round symbols in the box and whisker plots represent outliers that have exceeded the whisker values. Third, Kruskal-Wallis one-way ANOVA tests were performed between multiple time points (0, 1, 2, 4, 8, and 12-wks post-RTx) for a given bone surface and bone compositional parameter. Results were considered statistically significant at the $p < 0.05$ level.

3. Results

3.1. Cortical mineral/matrix ratios decrease progressively with post-RTx time

To determine whether cortical mineral/matrix ratios obtained from the tibial metaphyseal region declined following irradiation exposure, median percentage differences in mineral/matrix ratios obtained between irradiated (RTx, 4 × 5 Gy) and non-irradiated (non-RTx, 0 Gy) groups were examined by bone surface and post-RTx time. Mineral/matrix ratios were significantly decreased in endosteal and mid-cortical bone at 2-wks post-RTx (−16.9 and −7.5% respectively, $p < 0.05$ by Wilcoxon signed rank test), and periosteal bone by 4-wks post-RTx (−6.2%, $p < .05$) compared to age-matched non-RTx controls (Fig. 1). Significant differences in mineral/matrix ratios were also detected in the mid-cortical bone at 8-wks post-RTx (−9.3%, $p < 0.05$); and endosteal, mid-cortical, and periosteal bone at 12-wks post-RTx (−4.1, −8.7, and −5.1% respectively, $p < 0.05$). When pooled mineral/matrix ratio values were compared by time point, they were significantly reduced at 2, 4, 8, and 12-wks post-RTx (−7.5, −5.4, −7.7, and −8.3% respectively, $p < 0.05$) compared to the non-RTx controls and to 0 and 1-wk post-RTx (−2.6 and −0.4% respectively, $p < 0.05$). No significant differences in percent difference in mineral/matrix ratios were found between time points for a given bone surface using one-way ANOVA.

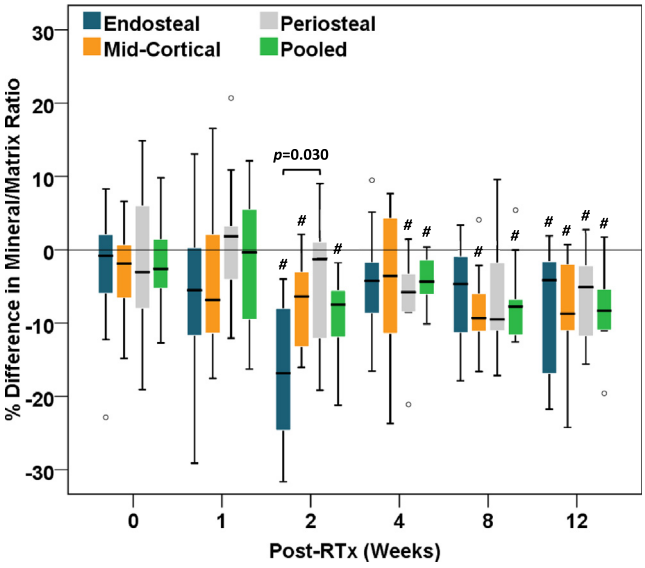

Fig. 1. Box and whisker plot represent the percent differences in mineral/matrix ratios between irradiated and non-irradiated specimens by cortical bone site and time post-RTx. Negative percentages indicate reduced bone mineral/matrix ratios. Statistically significant percent differences are shown by the # symbol at the $p < 0.05$ level (pair-wise comparison with related-samples Wilcoxon signed rank test). Statistically significant spatial differences between endosteal, mid-cortical, and/or periosteal bone surfaces are indicated by the p-value on the box and whisker plots (Kruskal-Wallis one-way ANOVA multi-group comparison test). Open circles represent outliers that have exceeded the whisker values.

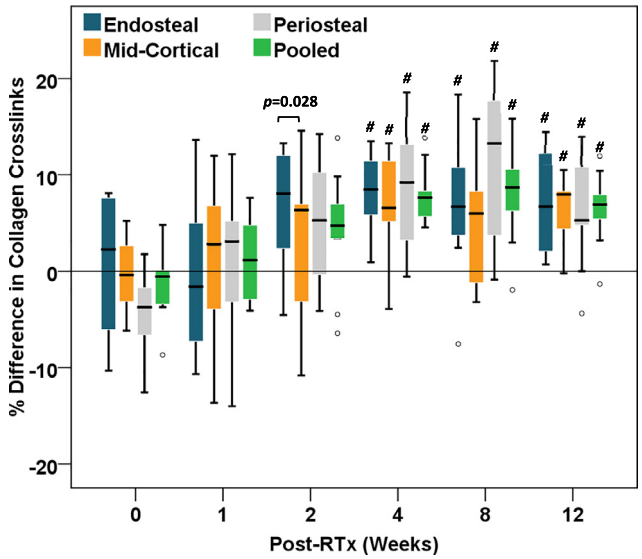

Fig. 2. Box and whisker plots representing the percent differences in collagen crosslinks ratios between irradiated and non-irradiated specimens by cortical bone site and time post-RTx. Positive percentages indicate increased bone collagen crosslinks ratios. Statistically significant percent differences are shown by the # symbol at the $p < 0.05$ level (pair-wise comparison with related-samples Wilcoxon signed rank test). Statistically significant spatial differences between endosteal, mid-cortical, and/or periosteal bone sites are indicated by the p-value on the box and whisker plots (Kruskal-Wallis one-way ANOVA multi-group comparison test). Open circles represent outliers that have exceeded the whisker values.

3.2. Cortical collagen crosslink ratios increase progressively with post-RTx time

No significant between-group percentage differences in collagen crosslinks ratios by bone surface were found at 0, 1, or 2-wks post-RTx (Fig. 2). However, collagen crosslinks ratios were significantly increased in endosteal, mid-cortical, and periosteal bone at 4-wks post-RTx (8.5, 6.6, and 9.2% respectively, $p < 0.05$ by Wilcoxon signed rank test). Collagen crosslinks ratios were also significantly increased in endosteal and periosteal bone at 8-wks post-RTx (6.7 and 13.3% respectively, $p < 0.05$); and endosteal, mid-cortical, and periosteal bone at 12-wks post-RTx (6.7, 8.0, and 5.3% respectively, $p < 0.05$). When pooled collagen crosslinks ratios were examined, they were only significantly increased at 4, 8, and 12-wks post-RTx (7.6, 8.7, and 6.9% respectively, $p < 0.05$). When percent difference in collagen crosslink ratios were examined between multiple time points by one-way ANOVA, significant differences ($p < 0.05$) were found between 0 vs. 2- or 4-wks and 1 vs. 2 or 4-wks for endosteal bone (Table S1). Similarly, significant differences in periosteal collagen crosslinks were found between 0 vs. 2, 4, 8, or 12-wks, 1 vs. 4 or 8-wks, and 2 vs. 8 wks (Table S1).

3.3. Cortical mineral crystallinity and Hyp/Pro ratios did not change with post-RTx time

The percent differences in mineral crystallinity between RTx and non-RTx groups are shown as a function of bone surface and post-RTx time point in Fig. 3. Positive percent changes would indicate increased mineral crystal maturity due to increased mineral crystal size and/or lattice perfection (Awonusi et al., 2007; Freeman et al., 2001). However, no significant percent differences in mineral crystallinity were found by bone site or time post-RTx. To determine whether bone collagen content in irradiated tibiae was also affected, the ratio of collagen-specific hydroxyproline (Hyp) and proline (Pro) bands or Hyp/Pro ratios were examined (Burke et al., 2016). Hyp/Pro ratios have been used as an indicator of post-translational modifications to collagen due to the enzymatic conversion of proline to hydroxyproline (Burke et al., 2016; Unal et al., 2018a; Buckley et al., 2012). In Fig. 4, Negative percent changes in Hyp/Pro ratios would indicate decreased proline hydroxylation, while positive percent changes would indicate either increased proline hydroxylation or increased collagen glycation (Unal et al., 2018a; Buckley et al., 2012). No significant percent differences in cortical Hyp/Pro ratios were found between RTx and non-RTx groups by bone surface or post-RTx time point. h.

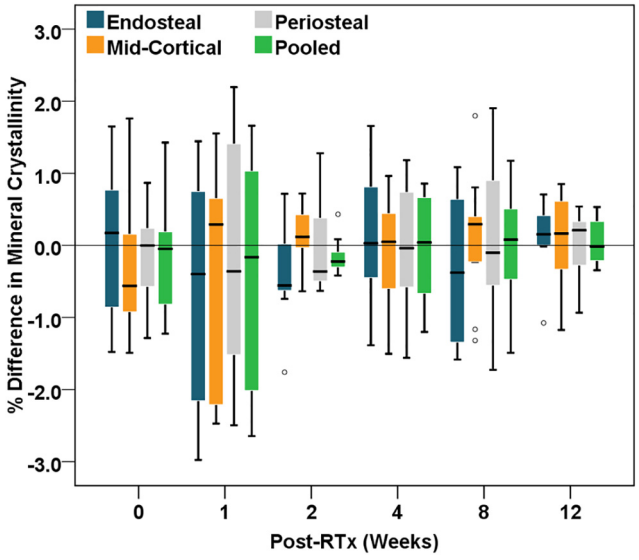

Fig. 3. Box and whisker plots representing the percent differences in mineral crystallinity between irradiated and non-irradiated groups by cortical bone site and time post-RTx. Positive percentages indicate increased mineral crystallinity. No statistically significant percent differences in mineral crystallinity were found between the groups at the $p < 0.05$ level (pair-wise comparison with related-samples Wilcoxon signed rank test). No statistically significant spatial differences were found between endosteal, mid-cortical, and/or periosteal bone sites at the $p < 0.05$ level (Kruskal-Wallis one-way ANOVA multigroup comparison test). Open circles represent outliers that have exceeded the whisker values.

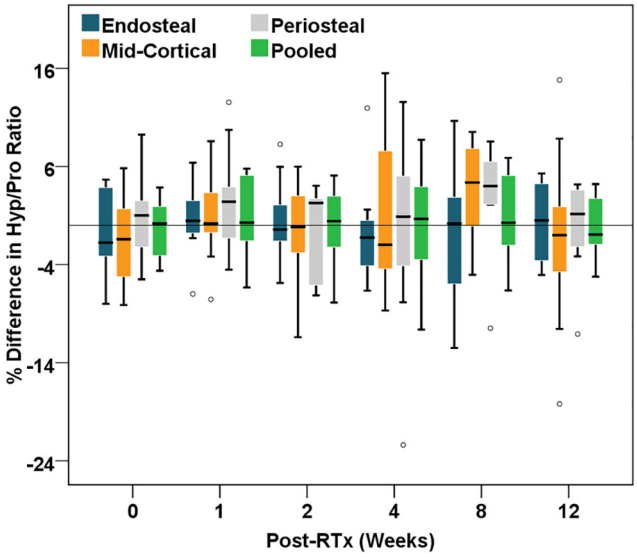

Fig. 4. Box and whisker plots representing the percent differences in Hyp/Pro ratios between irradiated and non-irradiated groups by cortical bone site and time post-RTx. Positive percentages indicate increased collagen proline hydroxylation. No statistically significant percent differences in Hyp/Pro ratios were found between the groups at the $p < 0.05$ level (pair-wise comparison with related-samples Wilcoxon signed rank test). No statistically significant spatial differences were found between endosteal, mid-cortical, and/or periosteal bone sites at the $p < 0.05$ level (Kruskal-Wallis one-way ANOVA multigroup comparison test). Open circles represent outliers that have exceeded the whisker values.

3.4. Irradiated endosteal bone exhibits the greatest spatial change in composition post-RTx

A significant percent difference in mineral/matrix ratio was found between endosteal vs. periosteal bone at 2-wks post-RTx (−16.9 vs. −1.3%, $p = 0.030$) using the Kruskal-Wallis one-way ANOVA comparison test (Table 1, Fig. 1). Similarly, a significant percent difference in collagen crosslinks ratio was found between endosteal vs. mid-cortical bone at 2-wks post-RTx (8.05 vs. 6.34%, $p = 0.028$) (Table 1, Fig. 2). When percent differences in mineral crystallinity (Fig. 3) and Hyp/Pro ratios (Fig. 4) were examined, no significant spatial differences were found between any of the bone surfaces.

When bone composition was examined within each experimental group, significant differences in mineral/matrix ratios were found in the RTx-group between endosteal vs. mid-cortical bone and endosteal vs. periosteal bone at 1-wk post-RTx (12.9 vs. 14.1 and 12.9 vs. 14.0, respectively, $p = 0.016$); and again at 2-wk post-RTx (12.3 vs. 13.7 and 12.3 vs. 14.0, respectively, $p = 0.047$) (Table 1, Fig. S1). A significant difference in mineral crystallinity was also found in the RTx-group between endosteal vs. mid-cortical bone at 2-wks post-RTx (0.0557 vs. 0.0562, respectively, $p = 0.049$ (Table 1, Fig. S3). For the non-RTx group, borderline to statistically significant spatial differences in mineral/matrix ratios were found between endosteal vs. mid-cortical bone at 0-wk post-RTx (14.2 vs. 15.1, respectively, $p = 0.024$); 1-wk post-RTx (13.6 vs. 14.9, respectively, $p = 0.058$); and 12-wks post-RTx (14.5

Table 1
Summary of select nonparametric Kruskal-Wallis multi-group comparison results obtained between bone surfaces across multiple time points (0, 1, 2, 4, 8, and 12-wks).

Experimental group	Time (weeks)	Compositional parameter	Comparison by bone surfaces	*p*-Value
RTx vs. non-RTx*	2	Mineral/matrix	Endo vs. Peri	0.030
RTx vs. non-RTx*	2	Collagen crosslinks	Endo vs. Mid	0.028
RTx	1	Mineral/matrix	Endo vs. Mid Endo vs. Peri	0.016
RTx	2	Mineral/matrix	Endo vs. Mid Endo vs. Peri	0.047
RTx	2	Crystallinity	Endo vs. Mid	0.049
Non-RTx	0	Mineral/matrix	Endo vs. Mid	0.024
Non-RTx	0	Crystallinity	Endo vs. Peri	0.066
Non-RTx	1	Mineral/matrix	Endo vs. Mid	0.058
Non-RTx	12	Mineral/matrix	Endo vs. Mid	0.004

* Percent difference between irradiated (4 × 5 Gy) and non-irradiated (0 Gy) groups. Endo = endosteal bone, Mid = mid-cortical bone, Peri = periosteal bone.

vs. 15.0, respectively, $p = 0.004$), respectively (Table 1, Fig. S1); whereas mineral crystallinity exhibited a borderline spatial difference between endosteal vs. periosteal bone at 0-wk post-RTx (0.0559 vs. 0.0563, respectively, $p = 0.058$) (Table 1, Fig. S3).

4. Discussion

The present study supports our hypothesis that irradiation with a fractionated 4 × 5Gy dose negatively impacts the composition of mouse tibial bone in a spatially and temporally-dependent manner, with metaphyseal endosteal cortical bone exhibiting the greatest change compared to periosteal or mid-cortical bone. The percent difference in mineral/matrix ratios was significantly reduced in endosteal bone compared to periosteal bone at 2-wks post-RTx ($p = 0.030$) (Table 1), while the percent difference in collagen crosslink ratios was significantly increased in endosteal bone compared to mid-cortical bone at 2-wks post-RTx ($p = 0.028$). When percent differences in mineral/matrix ratio were compared across time post-RTx, no significant differences were evident for any of the bone surfaces, suggesting that loss of spatial differences past 2 weeks is not the result of endosteal recovery. Endosteal and periosteal collagen crosslink ratios continued to increase (Fig. 1) and were significantly different between up to 4 weeks endosteally and up to 12 weeks periosteally (Table S1). Although not definitive, this suggests that the absence of significant percent differences at > 2 weeks post-RTx is more likely due to a different time course of periosteal response to RTx vs. endosteal, rather than a recovery of endosteal changes.

We hypothesize that the greatest change in mineral/matrix ratios found in irradiated endosteal bone (at 2-wks post-RTx) is attributed to its lower bone formation compared to periosteal bone. This hypothesis is supported by changes in endosteal cortical bone growth, composition, and mechanical properties reported in other studies involving hindlimb immobilization (Weinreb et al., 1991), mechanical loading (Brodt and Silva, 2010; De Souza et al., 2005), glucocorticoid treatment (Takahata et al., 2012), and a mouse model of senile osteoporosis (Silva et al., 2005). More importantly, our hypothesis is also supported by bone loss and bone formation studies performed on irradiated endosteal cortical bone (Sugimoto et al., 1991; Willey et al., 2010; Mustafy et al., 2018; Govey et al., 2016). For instance, in a female mouse 2 Gy irradiation model, bone formation rate per bone surface (BFR/BS) and mineralizing surface per bone surface (MS/BS) measurements were significantly reduced in irradiated endocortical bone compared to non-irradiated endocortical bone at 2-wks post-RTx, while no significant differences in BFR/BS or MS/BS measurements were reported between irradiated and non-irradiated periosteal bone at 2 or 3-wks post-RTx (Willey et al., 2010). Similarly, endosteal cortical bone formation and endosteal cortical bone thickness were significantly reduced within the tibial region of rabbits and mice after exposure to a single 50 or 10.75 Gy dose, respectively (Sugimoto et al., 1991; Govey et al., 2016).

In bone Raman spectroscopy, mineral crystallinity is associated with mineral crystal size and/or lattice perfection (Awonusi et al., 2007; Freeman et al., 2001), and therefore can provide information on bone growth, healing, or fragility fractures (Oest et al., 2015; Mandair and Morris, 2015). When percent differences in mineral crystallinity between the RTx and non-RTx groups were examined, no significant differences between the bone sites were found (Fig. 3). However, a borderline difference in mineral crystallinity was found in the RTx-group between endosteal and mid-cortical bone at 2-wks post-RTx ($p < 0.049$) (Fig. S3, Table 1). A non-significant trend towards a difference in mineral crystallinity between endosteal and mid-cortical bone was found in the non-RTx group at 0-wk post-RTx ($p < 0.066$). Nevertheless, the current result contrasts with our previous study in which a significant transient increase in mineral crystallinity was reported in the periosteum of irradiated tibias at 4-wks post-RTx (Oest et al., 2016). This discrepancy could be attributed to the inability of the FWHM metric to simultaneously distinguish between transient post-RTx changes in bone mineral crystallinity from non-resorbed older bone and recently deposited bone in a spatial manner.

The lower rate of bone formation hypothesized for irradiated endosteal bone could also account for the transient differences in collagen crosslinks ratios found between endosteal and mid-cortical bone at 2-wks post-RTx (Table 1, Fig. 2). The absence of significant differences between endosteal and periosteal bone was confounded by the variability in collagen crosslinks ratio measurements between experimental groups, especially within the RTx-group at 2, 4, and 8-wks post-RTx (Fig. 2, Fig. S2). Nevertheless, when percent differences in collagen crosslinks ratios were controlled for bone surface, they were significantly elevated across many of the irradiated bone surfaces at 4, 8, and 12-wks post-RTx. The findings of increased collagen crosslink ratios are consistent with other bone radiation studies (Oest et al., 2016; Chauhan et al., 2018), including our previous longitudinal post-RTx study performed on irradiated mouse tibias, whereby periosteal collagen crosslink ratios were persistently and significantly elevated for up to 26-wks post-RTx (Gong et al., 2013).

While these results provide compelling evidence for the temporal post-RTx accumulation of mature trivalent collagen crosslinks, quantification of each enzymatic crosslink was not biochemically evaluated by HPLC. The non-quantitative nature of localized Raman spectroscopic collagen crosslinks ratio measurements when compared to bulk HPLC measurements was previously highlighted in our lathyrism mouse model study (McNerny et al., 2015). Though some biochemical validation studies have been performed (Paschalis et al., 2001), interpretation of the band ratios underlying the amide-I region is still not thoroughly validated (McNerny et al., 2015; Gamsjaeger et al., 2017; Farlay et al., 2011). The absence of any significant percent changes in Hyp/Pro ratios between RTx and non-RTx groups with post-RTx time or bone surface (Fig. 3) suggests that post-translational modification of collagen was minimally impacted by the fractionated 4 × 5 Gy dose. While Hyp/Pro ratios were not calibrated to provide a direct measure of collagen content or proline hydroxylation for a given quantity of bone, a recent fluorometric study found that the collagen content of tibiae from mice irradiated with a fractionated 4 × 5 Gy dose was not significantly different from the collagen content of non-RTx tibiae between 1 and 12-wks post-RTx (Oest and Damron, 2014).

Although, cellular mechanisms of radiation-induced compositional changes have yet to be clarified, the early significant reduction in endosteal cortical mineral/matrix ratios found in this study could be attributed to increased osteoclastic bone resorption. Longitudinal single (5 Gy) and consecutive (4 × 5 Gy) mouse hindlimb irradiation studies have also reported transient increases in osteoclast numbers and activity within the metaphyseal region of irradiated femora at 2-wks post-

RTx (Oest et al., 2015). Similarly, whole-body mouse irradiation studies have demonstrated that the number and surface of tartrate-resistant acid phosphatase (TRAP) positive osteoclasts within the tibial metaphyseal region were also significantly elevated at 3 and 10-days post-RTx (Kondo et al., 2009). Osteoclast activity is elevated in circulating serum plasma of irradiated male mice at 2 and 10-days post-RTx (Green et al., 2013) and irradiated female mice at 1-wk post-RTx (Willey et al., 2010).

In contrast, interpreting the late stage decline in mineral/matrix ratios (8 and 12-wks post-RTx, Fig. S1) is complicated by the simultaneous interplay between long-term depletion of osteoclasts (Oest et al., 2015) and the delay in the recruitment and differentiation of new osteoblasts (Green and Rubin, 2014). The noticeable absence of a recovery in pooled cortical mineral/matrix ratios by 12-wks post-RTx (Fig. 1 and Fig. S1) suggests that bone adaptation was still primarily driven by osteoclastic bone resorption. Furthermore, the possibility of osteoblasts not being fully replenished by bone marrow-derived mesenchymal stem cells (MSCs) following radiation exposure could also be a significant factor. MSCs exposed to ionizing radiation may cause them to differentiate into adipocytes instead of osteoblasts (Green and Rubin, 2014), which may further delay the replenishing of osteoblast cell populations and the recovery of bone mineralization.

The recovery of bone composition at the irradiated endosteum may also be influenced by the post-RTx recovery of the adjacent bone marrow, which itself is negatively impacted by ionizing radiation (Green and Rubin, 2014). In a rabbit model, a synchronous partial recovery of both bone formation at the endosteum and hematopoietic cell numbers in the marrow were reported at 52-wks post-RTx, following a single 50 Gy dose (Sugimoto et al., 1991). Hematopoietic (stem) cells are necessary for the recovery of the irradiated marrow space, but these cells are also inhibited by the increased infiltration of adipocytes post-RTx (Green et al., 2013). Furthermore, tibial and femoral bone marrow lysates isolated from irradiated mice following a fractionated 4 × 5 Gy dose exhibited increased bone catabolic and decreased anabolic gene expression at 2–4 weeks post-RTx, followed by partial recovery (Oest et al., 2015), suggesting that bone cells near endosteal and trabecular surfaces were in communication with cells in the marrow space. Based on the studies summarized above, the endosteum is associated with reduced marrow osteoprogenitor cell numbers and impaired bone formation following irradiation (Silva et al., 2005). It is also clear that osteogenesis and adipogenesis are tightly regulated processes in irradiated animals, but whether the post-RTx recovery of the marrow space would also contribute to changes in bone composition, morphology, and function at the periosteum is unclear.

5. Strengths, limitations, and conclusions

The mouse model of limited field hindlimb irradiation utilized a standard protocol for the longitudinal evaluation of post-RTx changes to bone; however, some limitations need to be addressed. First, the use of transverse bone sections to compare the spatial differences in cortical bone composition across the tibial metaphyseal region has both strengths and weaknesses. One major strength of using transverse bone sections is that twice the number of endosteal, mid-cortical and periosteal bone surfaces can be sampled by Raman spectroscopy compared to using longitudinal bone sections. The decision to use transverse bone sections was based on prior histomorphometric studies in which the most significant changes in femoral bone modeling occurred within the proximal metaphyseal and mid-diaphyseal regions as opposed to the distal epiphyseal region (Oest et al., 2015; Oest et al., 2018). However, one limitation of using fresh transverse bone sections is the limited number of trabecular bone surfaces that are available for sampling by Raman spectroscopy. This situation is compounded by the fact that trabecular bone is more susceptible to radiation-induced osteoclastic bone resorption than cortical bone, and thus is more likely to be completely resorbed before the last post-RTx time point (Oest et al., 2018). For example, microCT images acquired from the femora following irradiation with a 4 × 5 Gy dose, exhibited complete loss in metaphyseal trabecular bone volume at 8, 12, and 26-wks post-RTx (Oest et al., 2018). For these reasons, spatial comparisons between trabecular and cortical bone composition were not examined in this current study.

Second, whole bone mechanical properties were not examined as part of this study. Notwithstanding, the mechanical strength and fracture toughness of cortical bone in the adjacent femur have been determined using the same longitudinal study design with this hindlimb irradiation model (McNerny et al., 2015; Rahman et al., 2018). A relative decrease in cortical tissue mineral density (TMD) in the irradiated mice at 4, 8, 12, and 26 weeks was paralleled by reduced flexural modulus and strength (McNerny et al., 2015). Interestingly, there was an immediate and sustained loss of bone fracture toughness (ability to resist crack propagation) persisting across all time points (Rahman et al., 2018). Both studies assume that the material properties through the bone cross-section are uniform, and this work suggests there may be some variation in mechanical properties through the cross section. The relative decrease in endosteal mineral/matrix ratio and increased collagen crosslink ratio would have a larger effect on the fracture toughness test because the crack front passes through all compartments of the cross section at all points during the crack propagation process. In contrast, strength properties derived from three-point bend tests are affected most by the periosteal bone because the highest stresses are located in that area. Material indentation methods could be used in the future to explore the spatial distribution of material properties as a result of therapeutic doses of irradiation.

Tibial bone bending strength is negatively impacted in irradiated rabbits at 12-wks post-RTx because of reduced endosteal cortical bone growth and increased cortical porosity (Sugimoto et al., 1991). In contrast, a 3-wk compressive loading stimulus applied to the tibiae of irradiated mice attenuates the loss of endosteal cortical bone thickness in vivo (Govey et al., 2016). We conjecture that the reduced cortical mineral/matrix ratios found in irradiated tibiae at 2, 4, 8, and 12-wks post-RTx in this study could also explain the increased incidences of post-RTx bone fragility fractures reported clinically. However, irradiation-induced changes in cortical mineral/matrix and collagen crosslinks ratios found in this study may not alone be sufficient to explain the mechanism of post-RTx bone embrittlement. Although not fully understood, post-RTx bone embrittlement is thought to be associated with the increased formation of non-enzymatic advanced glycation end-products or AGEs (Unal et al., 2018b; Bartlow et al., 2018). While AGEs, such as pentosidine, and other non-specific AGEs (nsAGEs) are increased within the femora of irradiated mice at 4-wks post-RTx, they could not alone account for the significant reduction in whole bone fracture toughness reported at 0, 4, and 12-Wks post-RTx (Bartlow et al., 2018). This suggests that post-RTx bone embrittlement may be driven by other bone compositional changes, such as collagen fragmentation (Bartlow et al., 2018; Rahman et al., 2018; Burton et al., 2014; Islam et al., 2016; Acill et al., 2007). This requires further investigation.

Third, the absence of significant spatial differences in mineral crystallinity between bone surfaces is unclear. Although, the tibiae used in this current study were controlled for mice age, information on bone tissue ages at endosteal, mid-cortical, and periosteal surfaces were not measured. The use of fluorochrome bone labels in the future could ensure that comparable mineral crystallinity measurements are obtained between experimental groups of similar bone ages (Sinder et al., 2016; Paschalis et al., 2017).

In conclusion, the results from this study support our hypothesis that limited field irradiation negatively impacts the composition of cortical bone in a spatially-dependent manner. Specifically, we report a significant early decline in endosteal mineral/matrix ratios and increased endosteal collagen crosslinks ratios at 2-wks post-RTx compared to periosteal and mid-cortical bone, respectively. When compositional measurements were pooled across the entire metaphyseal

cortex, mineral/matrix and collagen crosslink ratios were progressively impaired between 4, 8, and 12-wks post-RTx. These progressive post-RTx impairments to bone quality may contribute to the increased incidences of bone fragility fractures reported in clinical post-RTx patients (Hui et al., 2015; Mitchell and Logan, 1998; Damron, 2014). In contrast, no significant post-RTx spatial or progressive compositional differences in mineral crystallinity or collagen proline hydroxylation were found. The results from this study will be critical in evaluating the efficacy of pharmacologic interventions in counteracting the negative impacts of radiation on bone composition. Such studies would also benefit from additional correlative tissue-level bone quality and bone growth or nanoindentation analyses to clarify the mechanisms of post-RTx fragility fractures.

Transparency document

The Transparency document associated this article can be found, in online version.

Funding

This work was funded under NIH/NIAMS award #s R01 AR065419 (TAD), P30 AR069620 (DHK), and the David G. Murray Endowment from Upstate Medical University (TAD).

CRediT authorship contribution statement

Gurjit S. Mandair:Investigation, Formal analysis, Validation, Writing - original draft, Supervision.**Megan E. Oest**:Methodology, Investigation, Validation, Writing - original draft, Supervision.**Kenneth A. Mann**:Investigation, Validation, Writing - original draft, Supervision.**Michael D. Morris**:Methodology, Validation, Writing - original draft, Supervision.**Timothy A. Damron**:Methodology, Validation, Writing - original draft, Supervision.**David H. Kohn**:Validation, Writing - original draft, Supervision.

Declaration of competing interest

All authors state they have no conflicts of interest.

Appendix A. Supplementary data

Supplementary data to this article can be found online at https://doi.org/10.1016/j.bonr.2020.100262.

References

Acill, Y., Springer, I.N., Niehoff, P., Gassling, V., Warnke, P.H., Acmaz, S., Sonmez, T.T., Kimmig, B., Lefteris, V., Wiltfang, J., 2007. Proof of direct radiogenic destruction of collagen in vitro. Strahlenther. Onkol. 183 (7), 374–379. https://doi.org/10.1007/s00066-007-1598-0.

Awonusi, A., Morris, M.D., Tecklenburg, M.M.J., 2007. Carbonate assignment and calibration in the Raman spectrum of apatite. Calcif. Tissue Int. 81 (1), 46–52. https://doi.org/10.1007/s00223-007-9034-0.

de Baere, T., Tselikas, L., Gravel, G., Hakime, A., Deschamps, F., Honore, C., Mir, O., Lecesne, A., 2018. Interventional radiology: role in the treatment of sarcomas. Eur. J. Cancer 94, 148–155. https://doi.org/10.1016/j.ejca.2018.02.017.

Bartlow, C.M., Mann, K.A., Damron, T.A., Oest, M.E., 2018. Limited field radiation therapy results in decreased bone fracture toughness in a murine model. PLoS One 13 (10), e0204928. https://doi.org/10.1371/journal.pone.0204928.

Baxter, N.N., Habermann, E.B., Tepper, J.E., Durham, S.B., Virnig, B.A., 2005. Risk of pelvic fractures in older women following pelvic irradiation. JAMA 294 (20), 2587–2593. https://doi.org/10.1001/jama.294.20.2587.

Brodt, M.D., Silva, M.J., 2010. Aged mice have enhanced endocortical response and normal periosteal response compared with young-adult mice following 1 week of axial tibial compression. J. Bone Miner. Res. 25 (9), 2006–2015. https://doi.org/10.1002/jbmr.96.

Buckley, K., Matousek, P., Parker, A.W., Goodship, A.E., 2012. Raman spectroscopy reveals differences in collagen secondary structure which relate to the levels of mineralisation in bones that have evolved for different functions. J. Raman Spectrosc. 43 (9), 1237–1243. https://doi.org/10.1002/jrs.4038.

Burke, M.V., Atkins, A., Akens, M., Willett, T.L., Whyne, C.M., 2016. Osteolytic and mixed cancer metastasis modulates collagen and mineral parameters within rat vertebral bone matrix. J. Orthop. Res. 34 (12), 2126–2136. https://doi.org/10.1002/jor.23248.

Burton, B., Gaspar, A., Josey, D., Tupy, J., Grynpas, M.D., Willett, T.L., 2014. Bone embrittlement and collagen modifications due to high-dose gamma-irradiation sterilization. Bone 61, 71–81. https://doi.org/10.1016/j.bone.2014.01.006.

Cao, A., Pandya, A.K., Serhatkulu, G.K., Weber, R.E., Dai, H., Thakur, J.S., Naik, V.M., Naik, R., Auner, G.W., Rabah, R., Freeman, D.C., 2007. A robust method for automated background subtraction of tissue fluorescence. J. Raman Spectrosc. 38 (9), 1199–1205. https://doi.org/10.1002/jrs.1753.

Chauhan, S., Khan, S.A., Prasad, A., 2018. Irradiation-induced compositional effects on human bone after extracorporeal therapy for bone sarcoma. Calcif. Tissue Int. 103 (2), 175–188. https://doi.org/10.1007/s00223-018-0408-2.

Chen, H.H.W., Kuo, M.T., 2017. Improving radiotherapy in cancer treatment: promises and challenges. Oncotarget 8 (37), 62742–62758. https://doi.org/10.18632/oncotarget.18409.

Damron, T.A., 2014. CORR insights®: do long term survivors of Ewing family of tumors experience low bone mineral density and increased fracture risk? Clin. Orthop. Rel. Res. 472 (11), 3480–3482. https://doi.org/10.1007/s11999-014-3888-z.

De Souza, R.L., Matsuura, M., Eckstein, F., Rawlinson, S.C.F., Lanyon, L.E., Pitsillides, A.A., 2005. Non-invasive axial loading of mouse tibiae increases cortical bone formation and modifies trabecular organization: a new model to study cortical and cancellous compartments in a single loaded element. Bone 37 (6), 810–818. https://doi.org/10.1016/j.bone.2005.07.022.

Dickie, C.I., Parent, A.L., Griffin, A.M., Fung, S., Chung, P.W.M., Catton, C.N., Ferguson, P.C., Wunder, J.S., Bell, R.S., Sharpe, M.B., O'Sullivan, B., 2009. Bone fractures following external beam radiotherapy and limb-preservation surgery for lower extremity soft tissue sarcoma: relationship to irradiated bone length, volume, tumor location and dose. Int. J. Radiat. Oncol. Biol. Phys. 75 (4), 1119–1124. https://doi.org/10.1016/j.ijrobp.2008.12.006.

Dunlap, N.E., Cai, J., Biedermann, G.B., Yang, W.S., Benedict, S.H., Sheng, K., Schefter, T.E., Kavanagh, B.D., Larner, J.M., 2010. Chest wall volume receiving > 30 Gy predicts risk of severe pain and/or rib fracture after lung stereotactic body radiotherapy. Int. J. Radiat. Oncol. Biol. Phys. 76 (3), 796–801. https://doi.org/10.1016/j.ijrobp.2009.02.027.

Farlay, D., Duclos, M.E., Gineyts, E., Bertholon, C., Viguet-Carrin, S., Nallala, J., Sockalingum, G.D., Bertrand, D., Roger, T., Hartmann, D.J., Chapurlat, R., Boivin, G., 2011. The ratio 1660/1690 cm^{-1} measured by infrared microspectroscopy is not specific of enzymatic collagen cross-links in bone tissue. PLoS One 6 (12). https://doi.org/10.1371/journal.pone.0028736.

Freeman, J.J., Wopenka, B., Silva, M.J., Pasteris, J.D., 2001. Raman spectroscopic detection of changes in bioapatite in mouse femora as a function of age and in vitro fluoride treatment. Calcif. Tissue Int. 68 (3), 156–162. https://doi.org/10.1007/s002230001206.

Gamsjaeger, S., Robins, S.P., Tatakis, D.N., Klaushofer, K., Paschalis, E.P., 2017. Identification of pyridinoline trivalent collagen cross-links by Raman microspectroscopy. Calcif. Tissue Int. 100 (6), 565–574. https://doi.org/10.1007/s00223-016-0232-5.

Gong, B., Oest, M.E., Mann, K.A., Damron, T.A., Morris, M.D., 2013. Raman spectroscopy demonstrates prolonged alteration of bone chemical composition following extremity localized irradiation. Bone 57 (1), 252–258. https://doi.org/10.1016/j.bone.2013.08.014.

Govey, P.M., Zhang, Y., Donahue, H.J., 2016. Mechanical loading attenuates radiation-induced bone loss in bone marrow transplanted mice. PLoS One 11 (12), e0167673. https://doi.org/10.1371/journal.pone.0167673.

Green, D.E., Rubin, C.T., 2014. Consequences of irradiation on bone and marrow phenotypes, and its relation to disruption of hematopoietic precursors. Bone 63, 87–94. https://doi.org/10.1016/j.bone.2014.02.018.

Green, D.E., Adler, B.J., Chan, M.E., Lennon, J.J., Acerbo, A.S., Miller, L.M., Rubin, C.T., 2013. Altered composition of bone as triggered by irradiation facilitates the rapid erosion of the matrix by both cellular and physicochemical processes. PLoS One 8 (5), e64952. https://doi.org/10.1371/journal.pone.0064952.

Haas, R.L., Gronchi, A., van de Sande, M.A.J., Baldini, E.H., Gelderblom, H., Messiou, C., Wardelmann, E., Le Cesne, A., 2018. Perioperative management of extremity soft tissue sarcomas. J. Clin. Oncol. 36 (2), 118–124. https://doi.org/10.1002/cncr.28715.

Helmstedter, C.S., Goebel, M., Zlotecki, R., Scarborough, M.T., 2001. Pathologic fractures after surgery and radiation for soft tissue tumors. Clin. Orthop. Relat. Res. 389, 165–172.

Hui, S.K., Arentsen, L., Wilcox, A., Shanley, R., Yee, D., Ghebre, R., 2015. Spatial and temporal fracture pattern in breast and gynecologic cancer survivors. J. Cancer 6 (1), 66–69. https://doi.org/10.7150/jca.10288.

Ikushima, H., Osaki, K., Furutani, S., Yamashita, K., Kishida, Y., Kudoh, T., Nishitani, H., 2006. Pelvic bone complications following radiation therapy of gynecologic malignancies: clinical evaluation of radiation-induced pelvic insufficiency fractures. Gynecol. Oncol. 103 (3), 1100–1104. https://doi.org/10.1016/j.ygyno.2006.06.038.

Islam, A., Chapin, K., Moore, E., Ford, J., Rimnac, C., Akkus, O., 2016. Gamma radiation sterilization reduces the high-cycle fatigue life of allograft bone. Clin. Orthop. Rel. Res. 474 (3), 827–835. https://doi.org/10.1007/s11999-015-4589-y.

Jegoux, F., Malard, O., Goyenvalle, E., Aguado, E., Daculsi, G., 2010. Radiation effects on bone healing and reconstruction: interpretation of the literature. Oral Surg. Oral Med. Oral Pathol. Oral Radiol. Endod. 109 (2), 173–184. https://doi.org/10.1016/j.tripleo.2009.10.001.

Karampas, I.A., Orkoula, M.G., Kontoyannis, C.G., 2013. A quantitative bioapatite/

collagen calibration method using Raman spectroscopy of bone. J. Biophotonics 6 (8), 573–586. https://doi.org/10.1002/jbio.201200053.
Kazanci, M., Roschger, P., Paschalis, E.P., Klaushofer, K., Fratzl, P., 2006. Bone osteonal tissues by Raman spectral mapping: orientation-composition. J. Struct. Biol. 156 (3), 489–496. https://doi.org/10.1016/j.jsb.2006.06.011.
Kazanci, M., Wagner, H.D., Manjubala, N.I., Gupta, H.S., Paschalis, E., Roschger, P., Fratzl, P., 2007. Raman imaging of two orthogonal planes within cortical bone. Bone 41 (3), 456–461. https://doi.org/10.1016/j.bone.2007.04.200.
Kondo, H., Searby, N.D., Mojarrab, R., Phillips, J., Alwood, J., Yumoto, K., Almeida, E.A.C., Limoli, C.L., Globus, R.K., 2009. Total-body irradiation of postpubertal mice with ^{137}Cs acutely compromises the microarchitecture of cancellous bone and increases osteoclasts. Radiat. Res. 171 (3), 283–289. https://doi.org/10.1667/rr1463.1.
Kumar, S., Verma, T., Mukherjee, R., Ariese, F., Somasundaram, K., Umapathy, S., 2016. Raman and infra-red microspectroscopy: towards quantitative evaluation for clinical research by ratiometric analysis. Chem. Soc. Rev. 45 (7), 1879–1900. https://doi.org/10.1039/c5cs00540j.
Kwon, J.W., Huh, S.J., Yoon, Y.C., Choi, S.-H., Jung, J.Y., Oh, D., Choe, B.K., 2008. Pelvic bone complications after radiation therapy of uterine cervical cancer: evaluation with MRI. AJR Am. J. Roentgenol. 191 (4), 987–994. https://doi.org/10.2214/ajr.07.3634.
Mandair, G.S., Morris, M.D., 2015. Contributions of Raman spectroscopy to the understanding of bone strength. BoneKEy Rep 4. https://doi.org/10.1038/bonekey.2014.115.
Mandair, G.S., Steenhuis, P., Ignelzi Jr., M.A., Morris, M.D., 2018. Bone quality assessment of osteogenic cell cultures by Raman microscopy. J. Raman Spectrosc. 1–11. https://doi.org/10.1002/jrs.5521.
Mattes, M.D., Patel, K.R., Burt, L.M., Hirsch, A.E., 2016. A nationwide medical student assessment of oncology education. J. Cancer Educ. 31 (4), 679–686. https://doi.org/10.1007/s13187-015-0872-6.
McNerny, E.M.B., Gong, B., Morris, M.D., Kohn, D.H., 2015. Bone fracture toughness and strength correlate with collagen cross-link maturity in a dose-controlled lathyrism mouse model. J. Bone Miner. Res. 30 (3), 446–455. https://doi.org/10.1002/jbmr.2356.
Mitchell, M.J., Logan, P.M., 1998. Radiation-induced changes in bone. Radiographics 18 (5), 1125–1136. https://doi.org/10.1148/radiographics.18.5.9747611.
Mustafy, T., Benoit, A., Londono, I., Moldovan, F., Villemure, I., 2018. Can repeated in vivo micro-CT irradiation during adolescence alter bone microstructure, histomorphometry and longitudinal growth in a rodent model? PLoS One 13 (11), e0207323. https://doi.org/10.1371/journal.pone.027323.
Oest, M.E., Damron, T.A., 2014. Focal therapeutic irradiation induces an early transient increase in bone glycation. Radiat. Res. 181 (4), 439–443. https://doi.org/10.1667/rr13451.1.
Oest, M.E., Franken, V., Kuchera, T., Strauss, J., Damron, T.A., 2015. Long-term loss of osteoclasts and unopposed cortical mineral apposition following limited field irradiation. J. Orthop. Res. 33 (3), 334–342. https://doi.org/10.1002/jor.22761.
Oest, M.E., Gong, B., Esmonde-White, K., Mann, K.A., Zimmerman, N.D., Damron, T.A., Morris, M.D., 2016. Parathyroid hormone attenuates radiation-induced increases in collagen crosslink ratio at periosteal surfaces of mouse tibia. Bone 86, 91–97. https://doi.org/10.1016/j.bone.2016.03.003.
Oest, M.E., Policastro, C.G., Mann, K.A., Zimmerman, N.D., Damron, T.A., 2018. Longitudinal effects of single hindlimb radiation therapy on bone strength and morphology at local and contralateral sites. J. Bone Miner. Res. 33, 99–112. https://doi.org/10.1002/jbmr.3289.
Oh, D., Huh, S.J., 2014. Insufficiency fracture after radiation therapy. Radiat. Oncol. J. 32 (4), 213–220. https://doi.org/10.3857/roj.2014.32.4.213.
Orkoula, M.G., Vardaki, M.Z., Kontoyannis, C.G., 2012. Study of bone matrix changes induced by osteoporosis in rat tibia using Raman spectroscopy. Vib. Spectrosc. 63, 404–408. https://doi.org/10.1016/j.vibspec.2012.09.016.
Park, S.-H., Kim, J.-C., Lee, J.-E., Park, I.-K., 2011. Pelvic insufficiency fracture after radiotherapy in patients with cervical cancer in the era of PET/CT. Radiation Oncol. J. 29 (4), 269–276. https://doi.org/10.3857/roj.2011.29.4.269.
Paschalis, E.P., Verdelis, K., Doty, S.B., Boskey, A.L., Mendelsohn, R., Yamauchi, M., 2001. Spectroscopic characterization of collagen cross-links in bone. J. Bone Miner. Res. 16 (10), 1821–1828. https://doi.org/10.1359/jbmr.2001.16.10.1821.
Paschalis, E.P., Gamsjaeger, S., Klaushofer, K., 2017. Vibrational spectroscopic techniques to assess bone quality. Osteoporosis Int 28 (8), 2275–2291. https://doi.org/10.1007/s00198-017-4019-y.
Penel, G., Delfosse, C., Descamps, M., Leroy, G., 2005. Composition of bone and apatitic biomaterials as revealed by intravital Raman microspectroscopy. Bone 36 (5), 893–901. https://doi.org/10.1016/j.bone.2005.02.012.
Raghavan, M., Sahar, N.D., Wilson, R.H., Mycek, M.A., Pleshko, N., Kohn, D.H., Morris, M.D., 2010. Quantitative polarized Raman spectroscopy in highly turbid bone tissue. J. Biomed. Opt. 15 (3). https://doi.org/10.1117/1.3426310.
Rahman, N., Khan, R., Badshah, S., 2018. Effect of X-rays and gamma radiations on the bone mechanical properties: literature review. Cell Tissue Bank. 19 (4), 457–472. https://doi.org/10.1007/s10561-018-9736-8.
Rux, D.R., Song, J.Y., Pineault, K.M., Mandair, G.S., Swinehart, I.T., Schlientz, A.J., Garthus, K.N., Goldstein, S.A., Kozloff, K.M., Wellik, D.M., 2017. Hox11 function is required for region-specific fracture repair. J. Bone Miner. Res. 32 (8), 1750–1760. https://doi.org/10.1002/jbmr.3166.
Sa, Y., Guo, Y.R., Feng, X.W., Wang, M., Li, P., Gao, Y.X., Yang, X., Jiang, T., 2017. Are different crystallinity-index-calculating methods of hydroxyapatite efficient and consistent? New J. Chem. 41 (13), 5723–5731. https://doi.org/10.1039/c7nj00803a.
Shi, C., Mandair, G.S., Zhang, H.H., Vanrenterghem, G.G., Ridella, R., Takahashi, A., Zhang, Y.S., Kohn, D.H., Morris, M.D., Mishina, Y., Sun, H.C., 2018. Bone morphogenetic protein signaling through ACVR1 and BMPR1A negatively regulates bone mass along with alterations in bone composition. J. Struct. Biol. 201 (3), 237–246. https://doi.org/10.1016/j.jsb.2017.11.010.
Shimoyama, T., Katagiri, H., Harada, H., Murata, H., Wasa, J., Hosaka, S., Suzuki, T., Takahashi, M., Asakura, H., Nishimura, T., Yamada, H., 2017. Fracture after radiation therapy for femoral metastasis: incidence, timing and clinical features. J. Radiat. Res. 58 (5), 661–668. https://doi.org/10.1093/jrr/rrx038.
Silva, M.J., Brodt, M.D., Ko, M., Abu-Amer, Y., 2005. Impaired marrow osteogenesis is associated with reduced endocortical bone formation but does not impair periosteal bone formation in long bones of SAMP6 mice. J. Bone Miner. Res. 20 (3), 419–427. https://doi.org/10.1359/jbmr.041128.
Sinder, B.P., Lloyd, W.R., Salemi, J.D., Marini, J.C., Caird, M.S., Morris, M.D., Kozloff, K.M., 2016. Effect of anti-sclerostin therapy and osteogenesis imperfecta on tissue-level properties in growing and adult mice while controlling for tissue age. Bone 84, 222–229. https://doi.org/10.1016/j.bone.2016.01.001.
Sugimoto, M., Takahashi, S., Toguchida, J., Kotoura, Y., Shibamoto, Y., Yamamuro, T., 1991. Changes in bone after high-dose irradiation. Biomechanics and histomorphology. J. Bone Joint Surg. Br. 73 (3), 492–497.
Takahata, M., Maher, J.R., Juneja, S.C., Inzana, J., Xing, L., Schwarz, E.M., Berger, A.J., Awad, H.A., 2012. Mechanisms of bone fragility in a mouse model of glucocorticoid-treated rheumatoid arthritis implications for insufficiency fracture risk. Arthritis Rheum. 64 (11), 3649–3659. https://doi.org/10.1002/art.34639.
Taylor, E.A., Lloyd, A.A., Salazar-Lara, C., Donnelly, E., 2017. Raman and Fourier transform infrared (FT-IR) mineral to matrix ratios correlate with physical chemical properties of model compounds and native bone tissue. Appl. Spectrosc. 71 (10), 2404–2410. https://doi.org/10.1177/0003702817709286.
Unal, M., Uppuganti, S., Leverant, C.J., Creecy, A., Granke, M., Voziyan, P., Nyman, J.S., 2018a. Assessing glycation-mediated changes in human cortical bone with Raman spectroscopy. J. Biophotonics 11 (8). https://doi.org/10.1002/jbio.201700352.
Unal, M., Creecy, A., Nyman, J.S., 2018b. The role of matrix composition in the mechanical behavior of bone. Curr. Osteoporos. Rep. 16 (3), 205–215. https://doi.org/10.1007/s11914-018-0433-0.
Voroney, J.P.J., Hope, A., Dahele, M.R., Purdy, T., Franks, K.N., Pearson, S., Cho, J.B.C., Sun, A., Payne, D.G., Bissonnette, J.P., Bezjak, A., Brade, A.M., 2009. Chest wall pain and rib fracture after stereotactic radiotherapy for peripheral non-small cell lung cancer. J. Thorac. Oncol. 4 (8), 1035–1037. https://doi.org/10.1097/JTO.0b013e3181ae2962.
Weinreb, M., Rodan, G.A., Thompson, D.D., 1991. Immobilization-related bone loss in the rat is increased by calcium deficiency. Calcif. Tissue Int. 48 (2), 93–100. https://doi.org/10.1007/bf02555873.
Willey, J.S., Livingston, E.W., Robbins, M.E., Bourland, J.D., Tirado-Lee, L., Smith-Sielicki, H., Bateman, T.A., 2010. Risedronate prevents early radiation-induced osteoporosis in mice at multiple skeletal locations. Bone 46 (1), 101–111. https://doi.org/10.1016/j.bone.2009.09.002.